

HighPGibbs, a Practical Tool for Fluid-Rock Thermodynamic Simulation in Deep Earth and Its Application on Calculating Nitrogen Speciation in Subduction Zone Fluids

Richen Zhong¹, Yanxia Li¹, Barbara Etschmann², Joël Brugger², Chang Yu¹, and Hao Cui¹

¹University of Science and Technology Beijing

²Monash University

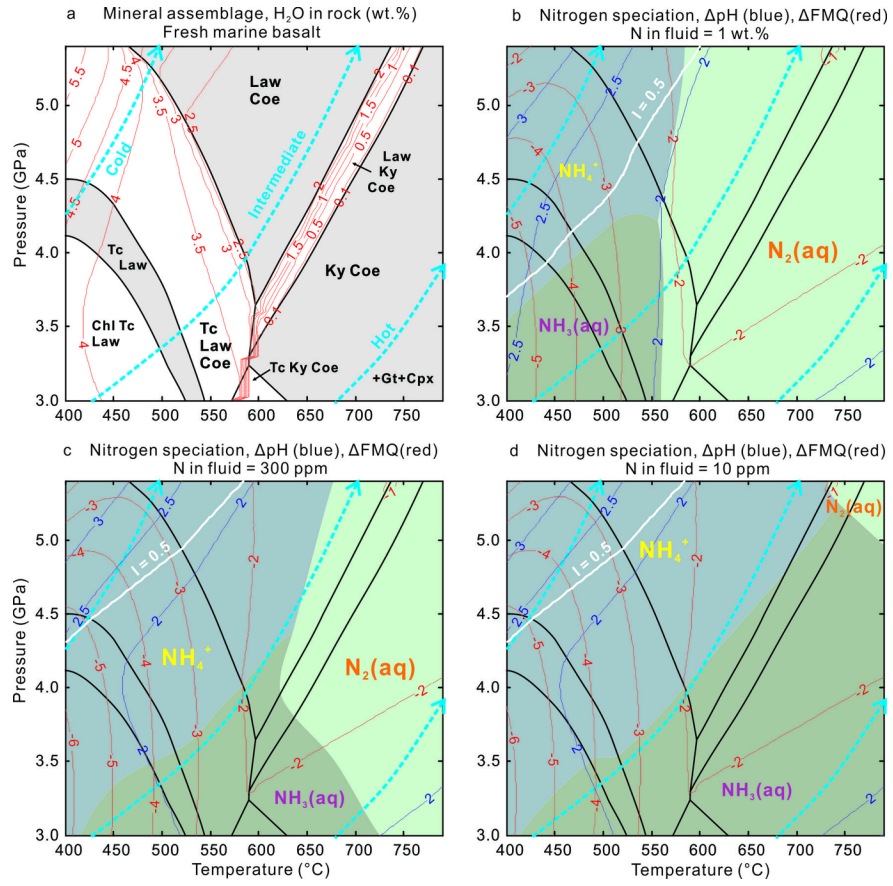
November 26, 2022

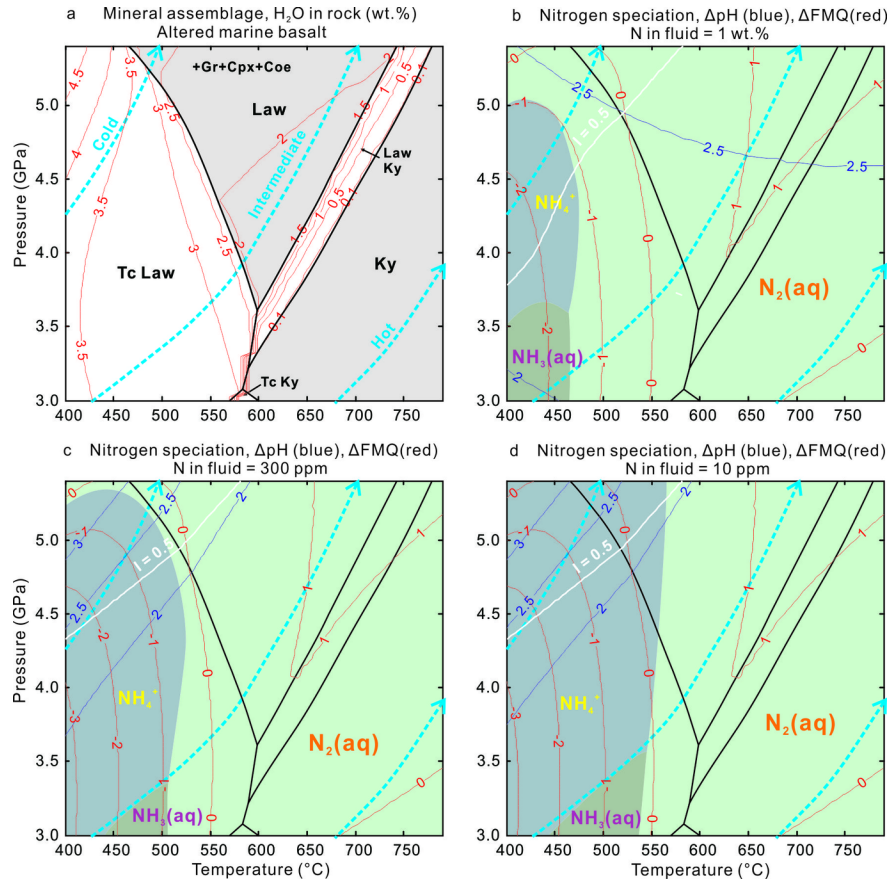
Abstract

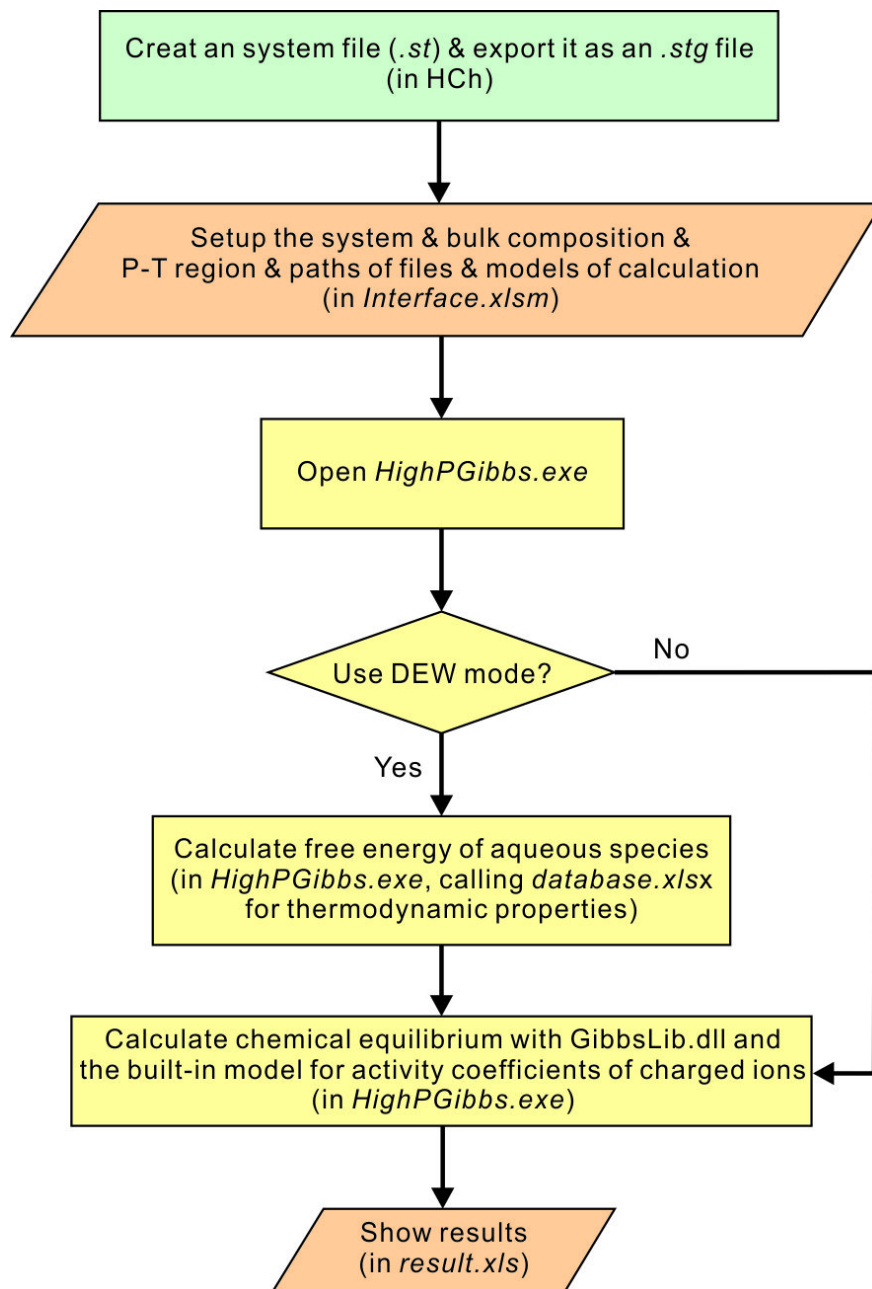
The HighPGibbs program is designed to calculate thermodynamic equilibrium of fluid-rock minerals and solid solutions up to depths of lithospheric mantle. It uses the Gibbs free energy minimization function of the HCh package to calculate mineral-fluid equilibrium assemblages. Chemical potentials of minerals are calculated using the equations of states included in HCh; free energy of aqueous species are calculated using the Deep Earth Water model; and activity coefficients of charged species are estimated using the Davies variant of the Debye-Hückel equation. HighPGibbs was applied to calculate nitrogen speciation in eclogite-buffered fluids from 400 to 790 °C and 30 to 54 kbar, to evaluate the mobility of nitrogen in subducting oceanic crust. Regardless of whether the protolith was altered (and oxidized) or not, N(aq) or NH(aq) are the predominant form of nitrogen in the slab-fluids at sub-arc temperatures, especially in cases of moderate or hot geotherms. Given that molecular nitrogen is highly incompatible in silicate minerals, the simulation indicates that nitrogen (as NH) in silicate minerals can be liberated during metamorphic devolatilization. The majority of nitrogen in subducting crusts can be unlocked during slab devolatilization and eventually expelled to the atmosphere via degassing of arc magmas. Therefore, oceanic crusts recycled to deep earth will be depleted in nitrogen compared to the newly formed crust at spreading centers. As a result of the long-term mantle convection, large proportions of the bulk silicate earth may have suffered nitrogen extraction via subduction, and this may account for the nitrogen enrichment in the Earth's atmosphere.

Hosted file

supporting-information 200209.docx available at <https://authorea.com/users/556394/articles/606429-highpgibbs-a-practical-tool-for-fluid-rock-thermodynamic-simulation-in-deep-earth-and-its-application-on-calculating-nitrogen-speciation-in-subduction-zone-fluids>







1 **HighPGibbs, a Practical Tool for Fluid-Rock Thermodynamic Simulation in Deep**
2 **Earth and Its Application on Calculating Nitrogen Speciation in Subduction Zone**
3 **Fluids**

4
5 **Richen Zhong**^{1*}, **Yanxia Li**¹, **Barbara Etschmann**², **Joël Brugger**^{2,3}, **Chang Yu**¹,
6 **Hao Cui**¹

7 ¹ Civil and Resource Engineering School, University of Science and Technology Beijing, Beijing
8 100083, China

9 ² School of Earth, Atmosphere and the Environment, Monash University, Clayton, Victoria
10 3800, Australia

11 ³ South Australian Museum, North Terrace, Adelaide, South Australia 5000, Australia

12
13
14 Corresponding author: Richen Zhong (zhongrichen@126.com)

15
16 **Key Points:**

- 17 • We present a thermodynamic tool that can simulate fluid-rock interaction at mantle
18 depths.
- 19 • Most nitrogen in subducting slabs can be liberated via slab devolatilization and
20 eventually expelled to the atmosphere.

22 **Abstract**

23 The HighPGibbs program is designed to calculate thermodynamic equilibrium of fluid-rock
24 minerals and solid solutions up to depths of lithospheric mantle. It uses the Gibbs free energy
25 minimization function of the HCh package to calculate mineral-fluid equilibrium assemblages.
26 Chemical potentials of minerals are calculated using the equations of states included in HCh; free
27 energy of aqueous species are calculated using the Deep Earth Water model; and activity
28 coefficients of charged species are estimated using the Davies variant of the Debye-Hückel
29 equation. HighPGibbs was applied to calculate nitrogen speciation in eclogite-buffered fluids
30 from 400 to 790 °C and 30 to 54 kbar, to evaluate the mobility of nitrogen in subducting oceanic
31 crust. Regardless of whether the protolith was altered (and oxidized) or not, N₂(aq) or NH₃(aq)
32 are the predominant form of nitrogen in the slab-fluids at sub-arc temperatures, especially in
33 cases of moderate or hot geotherms. Given that molecular nitrogen is highly incompatible in
34 silicate minerals, the simulation indicates that nitrogen (as NH₄⁺) in silicate minerals can be
35 liberated during metamorphic devolatilization. The majority of nitrogen in subducting crusts can
36 be unlocked during slab devolatilization and eventually expelled to the atmosphere via degassing
37 of arc magmas. Therefore, oceanic crusts recycled to deep earth will be depleted in nitrogen
38 compared to the newly formed crust at spreading centers. As a result of the long-term mantle
39 convection, large proportions of the bulk silicate earth may have suffered nitrogen extraction via
40 subduction, and this may account for the nitrogen enrichment in the Earth's atmosphere.

41 **Plain Language Summary**

42 Thermodynamic simulations are a powerful tool for investigating the geochemistry of fluid-rock
43 systems. Such simulations are difficult to perform when pressures are higher than 5 kbar. We
44 present a practical tool, HighPGibbs, that can calculate chemical equilibrium at pressures up to
45 ~55 kbar, and can be used to predict the behavior of mantle fluids. It was applied to calculate the
46 speciation of nitrogen in subduction zone fluids. The simulations show that molecular nitrogen,
47 which is incompatible in crustal rocks, is the predominant specie in most subduction zones
48 fluids. Therefore, most nitrogen in the subducting crusts can be unlocked by the fluids and
49 eventually released to the atmosphere via degassing of arc magmas.

50

51 **1. Introduction**

52 Thermodynamic modeling provides a powerful tool to understand the nature and evolution
53 of hydrothermal systems in the earth. The revised Helgeson–Kirkham–Flowers equation of state
54 (HKF EoS; [Tanger and Helgeson, 1988](#)) is widely used for equilibrium calculations of
55 hydrothermal systems, since it provides a self-consistent method to extrapolate the Gibbs free
56 energies of aqueous species at elevated pressures and temperatures (P-T), even for species where
57 high P-T experimental data are lacking. The validity of the original HKF EoS was limited to
58 pressures lower than 5 kbar due to limits in the equation of state of water, and therefore fluid
59 processes could only be simulated t the depths of middle crust or shallower. More recently, a
60 significant improvement of the HKF EoS, known as the Deep Earth Water (DEW) Model, was
61 proposed by [Sverjensky et al. \(2014\)](#). With the assistance of high-pressure water density ([Zhang
62 and Duan, 2005](#)) and dielectric constants ([Pan et al. 2013](#)) calculated by molecular dynamic
63 simulations, the DEW model extended the pressure range of the HKF EoS to up to 60 kbar,

64 equivalent to the depth of upper mantle. Moreover, a new method of extrapolating the stability of
65 aqueous species from ambient conditions to high pressures was proposed with the DEW model,
66 based mainly on the standard partial molar volume at room temperature. The model was coded as
67 an Excel spreadsheet along with a revised thermodynamic database of aqueous species (available
68 from [Sverjensky et al., 2014](#)). The spreadsheet calculates the standard partial molal Gibbs free
69 energies of aqueous species as well as changes in Gibbs free energy of reactions among aqueous
70 species, pure minerals, and gases at a given P-T, and was used to provide important insights in
71 the nature of mantle fluids, such as their ability to carry carbon ([Sverjensky et al., 2014b](#),
72 [Tumiati et al., 2017](#)) and nitrogen ([Mikhail and Sverjensky, 2014](#); [Mikhail et al. 2017](#)).

73 Hydrothermal activity at mantle depths, such as slab devolatilization and mantle
74 metasomatism, is characterized by high rock/fluid ratios and thus largely buffered by rock
75 mineralogy. Pioneering researches have investigated the geochemistry of rock-buffered fluids,
76 and provided important insights such as the redox and pH of deep fluids and their ability to
77 migrate rock-building lithophile elements (e.g., [Galvez et al., 2015, 2016](#); [Debret and Sverjensky,](#)
78 [2017](#)). However, integrating the DEW model in complex fluid-rock systems calculation,
79 especially those with solid solutions, remains challenging.

80 In this study, we introduce a practical and easy-to-use thermodynamic tool, HighPGibbs,
81 that solves geochemical equilibrium of complex fluid-rock systems including aqueous solution,
82 pure minerals and solid solutions at mantle pressures. HighPGibbs takes advantage of the Gibbs
83 energy minimization solver provided by the HCh software package ([Shvarov and Bastrakov,](#)
84 [1999](#)) to calculate chemical equilibrium of multiphase fluid-rock systems. Previous studies have
85 shown that the free energy minimization algorithm of HCh can well reproduce the geochemistry
86 of complex fluid-rock systems at low pressures (e.g., [Zhong et al., 2015](#); [Xing et al., 2019](#)). To

87 extend simulation to mantle depths, the DEW (Sverjensky et al., 2014) was coded in HighPGibbs,
88 together with the Davie variant of the Debye-Hückel equation for calculation of activities of
89 charged species in the electrolyte phase (Davies, 1962). The software calculates the distribution
90 of elements amongst the minerals and aqueous species included in the linked, fully editable
91 thermodynamic databases using an efficient implementation of the free energy minimization
92 algorithm. This enables geochemical calculations of fluid-rock systems, and the software makes
93 it easy to calculate element solubility and speciation over a P-T grid. A case study on the
94 speciation of aqueous nitrogen in subduction zone fluids carried out using HighPGibbs is
95 detailed in Section 3.

96 **2. The HighPGibbs program**

97 **2.1 General description**

98 The HighPGibbs program was developed based on HCh (Shvarov, 1999, 2008), and it reads
99 settings from, and outputs calculated results to, Excel spreadsheets. To use HighPGibbs, it is
100 necessary to install and register HCh and Microsoft Excel.

101 The HCh software package provides an ActiveX component, *GibbsLib.dll*, that calls the core
102 functions of HCh in the Visual Basic (VB) environment. This function allows replacement of the
103 free energies and activity coefficients of species with user-defined values, and then calculates
104 chemical equilibrium using a Gibbs energy minimization algorithm with these given values. The
105 VB-based software HighPGibbs takes advantage of this function; i.e., it calculates the high P-T
106 Gibbs free energies of formation for aqueous species using the DEW model (Sverjensky et al.,
107 2014), and then transfer these values to the free energy minimization solver of HCh.

108 After installation of HighPGibbs, a Microsoft Excel file (*database.xlsx*) and a HCh
109 Unitherm folder (*HighPUnitherm*) can be found in the root fold as the default database files (see

110 Supporting Information for details). For all minerals and aqueous species, the apparent standard
 111 molal Gibbs free energy of formation is defined as the difference between the Gibbs free energy
 112 of the mineral at a given P-T and those of the constituent elements at reference temperature
 113 (298.15 K) and pressure (1 bar). The thermodynamic properties of aqueous species are calculated
 114 using the built-in dataset of DEW, which were reevaluated and suitable for thermodynamic
 115 calculation at elevated pressures (Sverjensky et al., 2014). For pure minerals and solid solutions,
 116 the built-in HCh database, *Unitherm*, is used. The *Unitherm* database was updated with
 117 properties of key metamorphic minerals from Holland and Powell (1998) for thermodynamic
 118 modeling of fluid-rock systems.

119 Following the approach used by Galvez et al. (2015) to calculate activity coefficients of
 120 aqueous species at mantle pressures, the Davies variant of the Debye-Hückel law (Davies, 1962)
 121 was implemented to calculate the activity coefficients of charged ions (accurate to a ionic
 122 strength of ~0.5 molal; Bethke (2008)), and those of neutral species and water solvent are
 123 assumed to be unit. According to the Davies equation, the activity coefficient of j_{th} solute (γ_j) is:

$$124 \quad \log_{10}\gamma_j = \frac{-AZ_j^2\sqrt{I}}{1+\sqrt{I}} + 0.2AZ_j^2I \quad (1)$$

125 where I is the ionic strength of the solution and Z_j is the charge of j_{th} ion. A in Eq. 1 denotes the
 126 Debye-Hückel term that relates to the density ($\rho(P, T)$) and dielectric constant ($\epsilon(P, T)$) of pure
 127 water at elevated P-T:

$$128 \quad A = 1.82483 \cdot 10^6 \rho(P, T)^{0.5} (\epsilon(P, T) \cdot T)^{1.5} \quad (2)$$

129 where T is temperature in K, and I is the ionic strength,

$$130 \quad (3)$$

131

132 The activity coefficients depend on the ionic strength (I), which itself depends on the
133 molality of each solute in the solution (m_j in mol/kg H₂O). In HighPGibbs, the chemical
134 equilibrium is obtained by the following approach: (i) As a starting guess, the activity
135 coefficients of all aqueous species are given as the values that were optimized for the previous P-
136 T nodule, or assumed to be unit (for the first P-T nodule). The chemical equilibrium is then
137 calculated accordingly using the free energy minimization solver of HCh, yielding a calculated
138 composition and ionic strength (I) of the fluid. (ii) The activity coefficients of charged species
139 are calculated based on I , and the chemical equilibrium was re-calculated, yielding an updated
140 ionic strength (I'). (iii) Repeat (i) and (ii), until the result converges. In HighPGibbs, the
141 circulation stops when $(\frac{I-I'}{I'})^2 < 0.01$.

142 In this way, HighPGibbs can calculate the full distribution of species for a fluid-rock system
143 (with given bulk compositions) up to 60 kbar. The flow chart for calculating chemical
144 equilibrium using HighPGibbs is shown in [Figure 1](#), and details on running the program are
145 proved in the [Supporting Information](#). The install file and a tutorial can be found at
146 <http://47.93.192.148/download/Tutorial%20forHighPGibbs/Download.html> and Zenodo
147 (<https://zenodo.org/record/3660833#.XkEUwGgzZPY>).

148 **2.2 Limitations**

149 HighPGibbs uses the HCh built-in models to calculate the free energy of pure minerals and
150 solid solutions at elevated P-T. Compared with petrologic tools such as THERMOCALC, the
151 mineral models of HCh is less complex, lacking parameters to describe the thermal expansion
152 and compressibility of minerals, i.e., assuming the molar volumes of solids to be independent of
153 pressure and temperature. These yield differences between the mineral assemblages predicted
154 using HighPGibbs and those using THERMOCALC. Taking the breakdowns of two important

155 eclogite facies hydrous minerals (namely lawsonite and talc) for example, pseudosection of
156 marine basalt calculated using THERMOCALC yields a lawsonite-out temperature of ~ 770 °C at
157 4 GPa (Wei and Tian, 2014), whereas that predicted by HighPGibbs is ~ 730 °C at the same
158 pressure, using the same bulk composition. The talc-out temperature is calculated at ~ 620 °C at
159 4 GPa using THERMOCALC, and that is ~ 590 °C using HighPGibbs. Hence, HighPGibbs is not
160 suitable for barometry or thermometry. However, in calculating mineral solubilities at high
161 temperature, the properties of aqueous species are poorly known compared to those of minerals;
162 hence, the errors introduced by the simplification of mineral thermodynamics are acceptable.

163 The program typically fails to calculate chemical equilibrium under extreme P-T conditions.
164 In the case of calculating nitrogen speciation in eclogite-buffered fluids (see below), it solves the
165 fluid-rock equilibrium up to ~ 800 °C and ~ 55 kbar. Practically, fluids generated from subducting
166 basalts, greywackes or pelites behaves as supercritical fluids at pressures beyond that value, i.e.,
167 showing chemical continuum with silicate melts (Schmidt and Poli, 2014).

168 Finally, the Davies (1962) approach can well describe the activity coefficient of aqueous
169 species at ionic strength ≤ 0.5 molal. and the unit activity coefficient assumption for neutral
170 species and water solvent cannot be established for concentrated solutions. Therefore, cautions
171 should be paid when the calculated ionic strength is high.

172 **3. Application: speciation of aqueous nitrogen in subduction zone fluids**

173 **3.1 Geological background and method**

174 The speciation of aqueous nitrogen in the deep earth has control on the evolution of the
175 Earth's atmosphere. More specifically, if nitrogen exists predominantly as NH_4^+ , which is
176 moderately compatible in silicate minerals, it will be partly locked in the solid earth. In contrast,
177 it will be readily to be released into the atmosphere via degassing processes if it is mainly in the

178 form of $\text{N}_2(\text{aq})$ or $\text{NH}_3(\text{aq})$ (Mikhail and Sverjensky, 2014). A thermodynamic study of aqueous
179 speciation of nitrogen using the DEW model (Mikhail and Sverjensky, 2014) showed that in a
180 suprasubduction mantle wedge, which is more oxidized than upper mantle elsewhere, provides a
181 suitable environment to stabilize $\text{N}_2(\text{aq})$. The authors suggested that this accounts for the
182 enrichment of N_2 in the Earth's atmosphere.

183 Apart from mantle wedge redox, another factor that may influence the Earth's global budget
184 of nitrogen circulation is whether nitrogen in subducting slabs can be recycled into the Earth's
185 interior or released by slab fluids. To address this issue, Mikhail et al. (2017) calculated the
186 speciation of nitrogen in eclogite-buffered fluids at four individual P-T conditions (10 and
187 50 kbar, 600 and 1000 °C), showing that the subducting crust provides suitable pH and redox to
188 stabilize the mineralogically incompatible nitrogen species $\text{N}_2(\text{aq})$ or $\text{NH}_3(\text{aq})$, thus favoring
189 nitrogen liberation during devolatilization. These results demonstrated the importance of the
190 lithology of subducting rock, which buffers fluid pH and $f\text{O}_2(\text{g})$, in controlling the speciation of
191 aqueous nitrogen.

192 In this study, to better understand the nitrogen flux in subduction zones with varying thermal
193 structures, nitrogen speciation in basaltic eclogite-buffered fluids was calculated over a P-T grid
194 of 400 to 790 °C and 30 to 54 kbar (at increments of 10 °C and 0.25 kbar, respectively) in the Fe-
195 Mg-Na-Ca-Al-Si-O-H-N system. In subduction zones, thermal structure greatly influences the
196 amounts and depths of volatile liberation (e.g., Van Keken et al., 2011). Aside from the timing
197 and amounts of water solvent liberation, temperature has a first-order control in chemical
198 equilibrium, and thus the P-T conditions can significantly influence the speciation of volatiles.

199 To evaluate the influence of the rock's redox condition, two bulk compositions were used
200 for thermodynamic modeling, a fresh basalt at the ridge of the Pacific Ocean (sample PC CV 04

201 of Bézou and Humler, 2004) and the average of altered marine basalts at Pito Deep (Barker,
202 2010; Table 1). The calculations were carried out in the *Two-step Mode* of HighPGibbs (see
203 Supporting Information for details), in which the equilibrium calculation at each P-T point was
204 carried out as two steps: (i) The equilibrium of a solute-free system was calculated using the bulk
205 composition of 100 kg of basaltic rocks (Table 1) with excess amounts of water, to obtain the
206 water content that can stabilize the hydrous minerals in the metamorphic rock. (ii) Minor
207 amounts of free water with dissolved nitrogen (1 kg of water with 10^{-5} , 3×10^{-4} or 10^{-2} kg of
208 dissolved nitrogen) were added to the bulk composition of metamorphic rock obtained from
209 step 1, to obtain the speciation of aqueous nitrogen in eclogite-buffered fluids. Three different
210 bulk fluids compositions (with 10 ppm, 3000 ppm and 1 wt.% of dissolved nitrogen) were used
211 to evaluate the influence of bulk nitrogen concentration on nitrogen speciation (Mikhail et al.,
212 2017). Although the nitrogen concentrations in slab-fluids are poorly known, the broad range of
213 selected concentrations (from 10 ppm to 1 wt.%) is likely to cover those of natural slab-fluids
214 (Mikhail et al., 2017). A relatively low fluid/rock ratio (~ 0.01) was used for the calculation, to
215 simulate the rock-buffered nature of slab-fluids in subduction zones (Connolly and Galvez,
216 2018). In this approach, the speciation of nitrogen in slab-fluids is evaluated as a function of slab
217 P-T and the concentration of total fluid-borne nitrogen. The simulation reveals the compatibility
218 of nitrogen in subducting crusts with varying geotherms and thus whether it will be liberated via
219 devolatilization or recycled to deep earth.

220 The aqueous species involved in the simulation are listed in Table S1, and the sources of
221 their thermodynamic properties can be found in *database.xlsx* of the software package (see
222 Supporting Information for details), which includes the thermodynamic properties revised with
223 high-pressure experiment results by Sverjensky et al. (2014). The rock-building silicates and

224 oxides used in this simulation are from the database of [Holland and Powell \(1998\)](#), and the
225 involved minerals and the mixing models of solid solutions are listed in [Table S2](#). In this
226 simulation, the metamorphic rock buffers the redox and acidity of the slab-fluid, and thus
227 influences the speciation and mobility of aqueous nitrogen.

228 It is noted that nitrogen-bearing mineral end members are not included in the solid solutions,
229 and thus the nitrogen exchanges between minerals and aqueous species are neglected. Natural
230 eclogites host ppm-levels of nitrogen as substitution for K^+ in minerals such as phengite and
231 clinopyroxene ([Mikhail et al., 2017](#)). Given the high solubility of nitrogen in the form of $N_2(aq)$
232 or $NH_3(aq)$, the incompatible nitrogen can easily be leached by aqueous fluids (e.g., [Duan et al.,](#)
233 [2000](#)). As long as molecular nitrogen predominates, the efficiency of nitrogen liberation is likely
234 to be controlled mainly by the kinetics of the fluid-rock interaction (i.e., how effectively the K-
235 bearing minerals communicate with the metamorphic fluid) rather than the equilibrium between
236 mineralogically bound and aqueous nitrogen.

237 **3.2 Results and discussions**

238 The simulations show that dehydration of marine basalt at eclogite facies is controlled
239 mainly by breakdown of lawsonite and, to a lesser extent, talc and chlorite ([Figs. 2a and 3a](#)).
240 Two factors influencing the aqueous speciation of nitrogen, pH and $fO_2(g)$, are also shown as the
241 difference from neutral pH (defined as $\Delta pH = pH - pH_n$, where pH and pH_n denote the pH values
242 of the fluid and pure water, respectively) and the fayalite-magnetite-quartz buffer (ΔFMQ),
243 respectively ([Figs. 2 and 3](#)). The alkaline nature ($\Delta pH = 1.5$ to 3) of the eclogite-buffered fluid is
244 consistent with previous modeling results ([Galvez et al., 2016](#)). The reliability of the modeling
245 results can be evaluated by the simulated ionic strength of the fluid. Under most P-T conditions,
246 the simulated ionic strengths are between 0.1 and 0.3, well within the applicability of the Davies

247 equation ($I \leq 0.5$). The contour of $I = 0.5$ are also shown in [Figures 2 and 3](#), and the simulation
248 results with higher pressures and lower temperatures than the contour (at the upper left corner of
249 the P-T diagrams) yield ionic strength >0.5 and thus may not be accurate.

250 Consistent with previous modeling results ([Mikhail and Sverjensky, 2014; Mikhail et al.,](#)
251 [2017](#)), this study shows that the speciation of aqueous nitrogen is controlled mainly by the redox
252 and total nitrogen content of the slab-fluids. In altered marine basalts ([Figs. 2b-d](#)), which are
253 more oxidized than their unaltered precursors, $N_2(aq)$ predominates over reduced nitrogen
254 species ($NH_3(aq)$ and NH_4^+) in a broader P-T regime than that in fresh basalts ([Figs. 3b-d](#)). On
255 the other hand, in both altered and fresh basalts-buffered fluids, the predominant fields of $N_2(aq)$
256 shrinks with decreasing total nitrogen contents ([Figs, 2 and 3](#)).

257 In addition, temperature significantly controls the speciation of aqueous nitrogen speciation.
258 In general, higher temperature favors the stabilization of $N_2(aq)$ whereas as $NH_3(aq)$ or NH_4^+
259 predominate at lower temperatures ([Figs. 2 and 3](#)). For altered marine basalts, large amounts of
260 mineralogically bound water remained in the rock (~ 2.5 - 3.5 wt.%, mainly as lawsonite, [Figs. 2b-](#)
261 [d](#)) at temperatures where $N_2(aq)$ predominates in the fluids ($T > \sim 480$ - 550 °C). The result is
262 similar for the fresh basalts-buffered fluids with moderate or high contents of dissolved nitrogen.
263 In these scenarios, the eclogite retains of ~ 2.5 wt.% water in the P-T regimes of the predominant
264 fields of $N_2(aq)$ ($T > \sim 580$ - 650 °C; [Figs. 3b, c](#)). In the case of nitrogen-poor fluids (10 ppm of N,
265 [Fig. 3d](#)) buffered by fresh basalt, $NH_3(aq)$ predominates instead of $N_2(aq)$, when the rock
266 contains ~ 2 wt.% of mineralogically bound water as lawsonite.

267 Both $N_2(aq)$ and $NH_3(aq)$ are incompatible in silicate minerals and soluble in fluids, and
268 thus can be scavenged from the silicate minerals during subsequent dehydration of the down-
269 going oceanic crust (mainly by breakdown of lawsonite), regardless of the redox state of the

270 marine basalt. Given that molecular nitrogen is highly soluble in water under the P-T conditions
271 of interest (see Fig. 3 in Duan et al. (2000)), the majority of structurally bound nitrogen may
272 soon be leached out via dehydration of lawsonite. Furthermore, two processes may enhance the
273 liberation of nitrogen. First, the devolatilization reactions (e.g., lawsonite breakdown) involve
274 interactions amongst silicate minerals and destruction/reconstruction of crystal structures, a
275 process that facilitates nitrogen liberation from the structures of silicate crystals (Niedermeier et
276 al., 2009). Second, shear deformation accompanying metamorphism will facilitate
277 communication between metamorphic minerals and fluids (e.g., Tomkins et al., 2010).

278 Exceptions are subduction zones with cold geotherms (Figs. 2a, 3a), where a significant
279 amount of water can be retained to large depths (van Keken et al., 2011). In cases of fluids
280 buffered by fresh basalt (Figs. 3b-d) or with low nitrogen contents (Fig. 2d), NH_4^+ predominates
281 along the P-T path of the cold subduction zone and nitrogen in subducting basalt can be recycled
282 to deep earth. This may explain the observation of surface-sourced nitrogen in diamonds, which
283 requires nitrogen surviving subduction devolatilization and transportation to depths greater than
284 that of diamond stability (Mikhail et al., 2014), or even to lower mantle (Palot et al., 2012). We
285 speculate that this scenario is less common than nitrogen discharging in subduction zones. First,
286 the stability of NH_4^+ requires both unaltered protolith (except for the cases of very low contents
287 of dissolved nitrogen) and a cold subduction zone (Fig. 2). Second, oceanic crust will be
288 significantly enriched in nitrogen during submarine alteration (Bebout et al., 2016), and thus
289 altered crusts should have greater contributions to the global nitrogen circulation than their
290 unaltered precursors.

291 In most cases, nitrogen in a subducting crust is mainly in the form of $\text{N}_2(\text{aq})$ or $\text{NH}_3(\text{aq})$
292 under sub-arc P-T conditions, and thus it will be released to the mantle wedge and expelled to the

293 atmosphere via arc volcanism. If the subducting slab is hot enough, large amounts of water will
294 be released at shallower depths in fore arc regions (van Keken et al., 2011). In these cases,
295 massive amounts of nitrogen gas may also be released via fluid venting near a trench. This is
296 more likely to take place if the subducting crust was altered and oxidized, where $N_2(aq)$ begins to
297 predominate at lower temperatures (Fig. 2).

298 Combined with the incompatibility of nitrogen in a mantle wedge (Mikhail and Sverjensky,
299 2014), subduction zones provide a highway to transfer nitrogen from a subducting slab to the
300 atmosphere, in line with the geological observation in modern convergent margins (Fischer et al.,
301 2002). This implies not only a strong retention of nitrogen in the Earth's atmosphere, but also the
302 mechanism that controls the long-term global nitrogen circulation. The subduction factory works
303 as a filter that continuously intercepts nitrogen from incoming subducting crust, which was
304 originally derived from upwelling asthenosphere at spreading centers. In the perspective of
305 global plate tectonics, nitrogen is released to the atmosphere from not only the mantle wedge per
306 se, but also large volumes of lithosphere fed into subduction zones.

307 In most cases, incompatible molecular nitrogen will predominate over NH_4^+ , regardless of
308 whether the crust underwent submarine alteration or not (Figs. 2 and 3). Therefore, elevated
309 redox conditions are not necessary for the mobility of nitrogen during slab devolatilization,
310 suggesting that the “nitrogen filter” may have initiated as early as the onset of plate tectonics,
311 which may have been recycling crustal material for more than 3 billion years (e.g., Bizzarro et
312 al., 2002). Furthermore, the hot geotherm of early Precambrian eras would also enhance the
313 stability of $N_2(aq)$ or $NH_3(aq)$ (Figs. 2 and 3). As a result of the long-term mantle convection,
314 large portions of the Earth's crust and upper mantle may have been subjected to nitrogen
315 extraction by subduction, and this may account for the nitrogen enrichment of the Earth's

316 atmosphere compared to other terrestrial planets (Mikhail and Sverjensky, 2014). The simulation
317 suggests that plate tectonics results in a net outgassing flux of nitrogen into the atmosphere,
318 supporting the idea of increasing nitrogen in the Earth's atmosphere over geological time, a
319 hypothesis that is still debated (Zerle and Mikhail, 2017).

320

321 **4. Conclusions**

322 (1) The HighPGibbs software provides a practical tool to calculate chemical equilibrium of
323 complex fluid-rock systems involving aqueous fluids, simple minerals and solid solutions at
324 mantle depths, enabling quantitative assessment of complex fluid-rock interactions from the
325 surface to the mantle within a self-consistent framework.

326 (2) In most cases, aqueous nitrogen in slab-fluids is predominated by incompatible $N_2(aq)$ or
327 $NH_3(aq)$ under sub-arc P-T conditions and thus the majority of mineralogically bound nitrogen in
328 oceanic crusts will be expelled to the atmosphere via slab subduction.

329

330 **Acknowledgement**

331 The HighPGibbs program is available at Zenodo
332 (<https://zenodo.org/record/3660833#.XkEUwGgzZPY>). The data used for the thermodynamic
333 simulation are in Tables S1 and S2 and accessible at Zenodo
334 (<https://zenodo.org/record/3660412#.XkANjaEw-QI>). The comments of two anonymous
335 reviewers provided considerable assistance in improving the software and the original submitted
336 manuscript. This work is financially supported by the National Natural Science Foundation of
337 China (Nos. 41872078 and 41502069), the Australian Research Council (DP190100216), the

338 Young Elite Scientists Sponsorship Program by CAST (YESS), and the Fundamental Research
339 Funds for the Central Universities (No. FRF-TP-18-017A3).

340

341 **References**

342 Barker, A. K., Coogan, L. A., and Gillis, K. M., 2010. Insights into the behaviour of sulphur in
343 mid-ocean ridge axial hydrothermal systems from the composition of the sheeted dyke
344 complex at Pito Deep. *Chem Geol* 275, 105–115.

345 Bebout, G. E., Lazzeri, K. E., and Geiger, C. A., 2016. Pathways for nitrogen cycling in Earth's
346 crust and upper mantle: A review and new results for microporous beryl and cordierite. *Am*
347 *Mineral* 101, 7–24.

348 Bethke, C. M., 2008. *Geochemical and Biogeochemical Reaction Modeling*. Cambridge
349 University Press, New York.

350 Bézou, A. and Humler, E., 2005. The $\text{Fe}^{3+}/\Sigma\text{Fe}$ ratios of MORB glasses and their implications for
351 mantle melting. *Geochim Cosmochim Acta* 69, 711–725.

352 Bizzarro, M., Simonetti, A., Stevenson, R. K., and David, J., 2002. Hf isotope evidence for a
353 hidden mantle reservoir. *Geology* 30, 771–774.

354 Connolly, J. A. D. and Galvez, M. E., 2018. Electrolytic fluid speciation by Gibbs energy
355 minimization and implications for subduction zone mass transfer. *Earth Planet Sc Lett* 501,
356 90–102.

357 Davies, C. W., 1962. *Ion association*. Butterworths, London.

358 Debret, B. and Sverjensky, D. A., 2017. Highly oxidising fluids generated during serpentinite
359 breakdown in subduction zones. *Scientific Reports* 7, 10351.

- 360 Duan, Z., Møller, N., and Weare, J. H., 2000. Accurate prediction of the thermodynamic
361 properties of fluids in the system $\text{H}_2\text{O}-\text{CO}_2-\text{CH}_4-\text{N}_2$ up to 2000 K and 100 kbar from a
362 corresponding states/one fluid equation of state. *Geochim Cosmochim Acta* 64, 1069–1075.
- 363 Fischer, T. P., Hilton, D. R., Zimmer, M. M., Shaw, A. M., Sharp, Z. D., and Walker, J. A.,
364 2002. Subduction and recycling of nitrogen along the central American margin. *Science*
365 297, 1154–1157.
- 366 Galvez, M. E., Manning, C. E., Connolly, J. A. D., and Rumble, D., 2015. The solubility of rocks
367 in metamorphic fluids: A model for rock dominated conditions to upper mantle pressure and
368 temperature. *Earth Planet Sc Lett* 430, 486–498.
- 369 Galvez, M. E., Connolly, J., and Manning, C. E., 2016. Implications for metal and volatile cycles
370 from the pH of subduction zone fluids. *Nature* 539, 420–424.
- 371 Holland, T. J. B. and Powell, R., 1998. An internally consistent thermodynamic data set for
372 phases of petrological interest. *J Metamorph Geol* 16, 309–343.
- 373 Mikhail, S., Barry, P. H., and Sverjensky, D. A., 2017. The relationship between mantle pH and
374 the deep nitrogen cycle. *Geochim Cosmochim Acta* 209, 149–160.
- 375 Mikhail, S. and Sverjensky, D. A., 2014. Nitrogen speciation in upper mantle fluids and the
376 origin of Earth's nitrogen-rich atmosphere. *Nature Geoscience* 36, 1164–1167.
- 377 Mikhail, S., Verchovsky, A. B., Howell, D., Hutchison, M. T., Southworth, R., Thomson, A. R.,
378 Warburton, P., Jones, A. P., and Milledge, H. J., 2014. Constraining the internal variability
379 of the stable isotopes of carbon and nitrogen within mantle diamonds. *Chem Geol* 366, 14–
380 23.

- 381 Niedermeier, D. R., Putnis, A., Geisler, T., Golla-Schindler, U., and Putnis, C. V., 2009. The
382 mechanism of cation and oxygen isotope exchange in alkali feldspars under hydrothermal
383 conditions. *Contrib Mineral Petr* 157, 65–76.
- 384 Palot, M., Cartigny, P., Harris, J. W., Kaminsky, F. V., and Stachel, T., 2012. Evidence for deep
385 mantle convection and primordial heterogeneity from nitrogen and carbon stable isotopes in
386 diamond. *Earth Planet Sc Lett* 357, 179–193.
- 387 Pan, D., Spanu, L., Harrison, B., Sverjensky, D. A., and Galli, G., 2013. Dielectric properties of
388 water under extreme conditions and transport of carbonates in the deep Earth. *P Natl Acad
389 Sci Usa* 110, 6646–6650.
- 390 Schmidt, M. W. and Poli, S., 2014. Devolatilization during subduction. *Treatise on
391 Geochemistry* 4, 669–701.
- 392 Shvarov, Y., 1999. Algorithmization of the numeric equilibrium modeling of dynamic
393 geochemical processes. *Geochem Int+* 37, 571–576.
- 394 Shvarov, Y., 2008. HCh: New potentialities for the thermodynamic simulation of geochemical
395 systems offered by windows. *Geochem Int+* 46, 834–83.
- 396 Sverjensky, D. A., Harrison, B., and Azzolini, D., 2014. Water in the deep Earth: The dielectric
397 constant and the solubilities of quartz and corundum to 60 kb and 1200 °C. *Geochim
398 Cosmochim Ac* 129, 125–145.
- 399 Tanger, J. C. and Helgeson, H. C., 1988. Calculation of the thermodynamic and transport
400 properties of aqueous species at high pressures and temperatures; revised equations of state
401 for the standard partial molal properties of ions and electrolytes. *Am J Sci* 288, 19–98.
- 402 Tomkins, A. G., 2010. Windows of metamorphic sulfur liberation in the crust: Implications for
403 gold deposit genesis. *Geochim Cosmochim Ac* 74, 3246–3259.

- 404 Tumiati, S., Tiraboschi, C., Sverjensky, D. A., Pettke, T., Recchia, S., Ulmer, P., Miozzi, F.,
405 and Poli, S., 2017. Silicate dissolution boosts the CO₂ concentrations in subduction fluids.
406 *Nature Communications* 8, 616.
- 407 van Keken, P. E., Hacker, B. R., Syracuse, E. M., and Abers, G. A., 2011. Subduction factory: 4.
408 Depth-dependent flux of H₂O from subducting slabs worldwide. *Journal of Geophysical*
409 *Research-Solid Earth* 116, B01401.
- 410 Wei, C. J. and Tian, Z. L., 2014. Modelling of the phase relations in high-pressure and ultrahigh-
411 pressure eclogites. *Isl Arc* 23, 254–262.
- 412 Xing, Y. L., Brugger, J., Tomkins, A., and Shvarov, Y., 2019. Arsenic evolution as a tool for
413 understanding formation of pyritic gold ores. *Geology* 47, 335–338.
- 414 Zerkle, A. L. and Mikhail, S., 2017. The geobiological nitrogen cycle: From microbes to the
415 mantle. *Geobiology* 15, 343–352.
- 416 Zhang, Z. and Duan, Z., 2005. Prediction of the PVT properties of water over wide range of
417 temperatures and pressures from molecular dynamics simulation. *Phys Earth Planet In* 149,
418 335–354.
- 419 Zhong, R. C., Brugger, J., Tomkins, A., Chen, Y. J., and Li, W. B., 2015. Fate of gold and base
420 metals during metamorphic devolatilization of a pelite. *Geochim Cosmochim Acta* 171, 338–
421 352.
- 422
- 423 **References from Supporting Information**
- 424 Green, E., Holland, T., and Powell, R., 2007. An order-disorder model for omphacitic pyroxenes
425 in the system jadeite-diopside-hedenbergite-acmite, with applications to eclogitic rocks. *Am*
426 *Mineral* 92, 1181-1189.

- 427 Holland, T. J. B. and Powell, R., 1998. An internally consistent thermodynamic data set for
428 phases of petrological interest. *J Metamorph Geol* 16, 309–343.
- 429 Powell, R. and Holland, T., 1999. Relating formulations of the thermodynamics of mineral solid
430 solutions: Activity modeling of pyroxenes, amphiboles, and micas. *Am Mineral* 84, 1–14.
- 431 White, R. W., Powell, R., and Holland, T. J. B., 2007. Progress relating to calculation of partial
432 melting equilibria for metapelites. *J Metamorph Geol* 25, 511-527.
- 433

434 **Figure Captions**

435

436 **Figure 1.** The flow chart of the HighPGibb. (Black-and-white in print)

437

438 **Figure 2.** Results of thermodynamic simulation for fluids buffered by eclogite metamorphosed
439 from altered marine basalt, showing P-T pseudosection showing mineral assemblage and
440 content of lithological bound water (a) and the Predominance fields of fluid-borne nitrogen in the
441 eclogite-buffered fluid with varying total nitrogen contents (b-d). The geotherms of hot,
442 intermediate and cold subduction zones are for slab Moho, from [van Keken et al. \(2011\)](#). Also
443 shown are the acidity (ΔpH , red lines with labels) and redox (ΔFMQ , blue) of the fluid. ΔpH is
444 the deviation of fluid pH from neutral pH (pH_n) ($\Delta\text{pH} = \text{pH} - \text{pH}_n$), and ΔFMQ the difference in
445 $\log f_{\text{O}_2(\text{g})}$ of the fluid relative to the fayalite-magnetite-quartz (FMQ) buffer ($\Delta\text{FMQ} = \log$
446 $f_{\text{O}_2(\text{g}),\text{fluid}} - \log f_{\text{O}_2,\text{FMQ}}$). The contour of ionic strength equal to 0.5 molal ($I = 0.5$) is shown and P-
447 T regime with higher pressures and lower temperatures than the contour have ionic higher than
448 this value. Bulk rock compositions used for simulation are given in [Table 1](#). Mineral
449 abbreviations: Opx = orthopyroxene; Cpx = clinopyroxene; Gt = garnet; Coe = coesite; Law =
450 lawsonite; Tc = talc; Ky = kyanite; Chl = chlorite. (Color in print).

451

452 **Figure 3.** The same as Fig. 2, but the composition of fresh marine basalt (see [Table 1](#)) was used
453 for the simulation. (Color in print)

454

455 **Table**

456

457

Table 1. Bulk rock compositions used in the modelling (in wt.%, H₂O in access)

	Altered marine	Fresh marine
	basalt	basalt
SiO ₂	52.03	50.12
Al ₂ O ₃	14.33	15.41
MgO	7.80	8.81
FeO	8.99	7.85
Fe ₂ O ₃	2.73	1.21
CaO	11.27	12.51
Na ₂ O	2.76	2.51

458

Figure 1.

Create a system file (.st) & export it as an .stg file
(in HCh)

Setup the system & bulk composition &
P-T region & paths of files & models of calculation
(in *Interface.xlsx*)

Open *HighPGibbs.exe*

Use DEW mode?

No

Yes

Calculate free energy of aqueous species
(in *HighPGibbs.exe*, calling *database.xlsx*
for thermodynamic properties)

Calculate chemical equilibrium with GibbsLib.dll and
the built-in model for activity coefficients of charged ions
(in *HighPGibbs.exe*)

Show results
(in *result.xls*)

Figure 2.

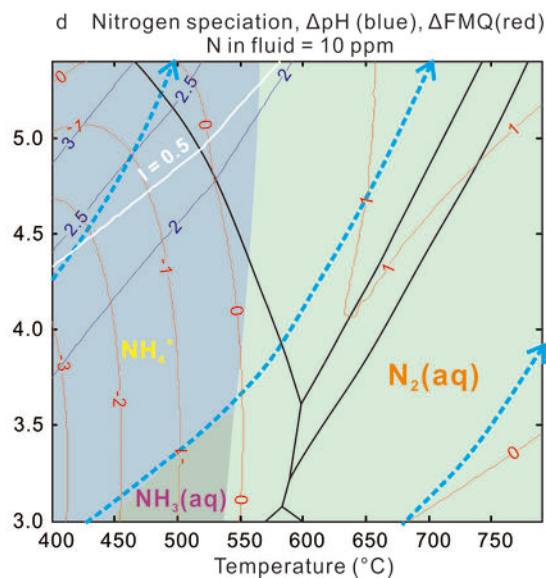
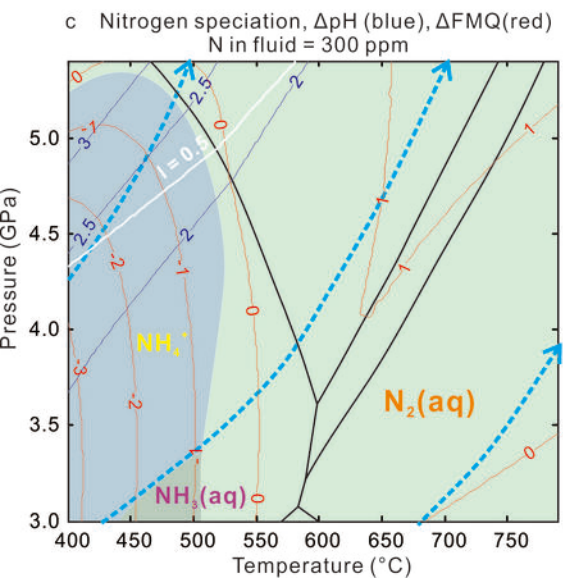
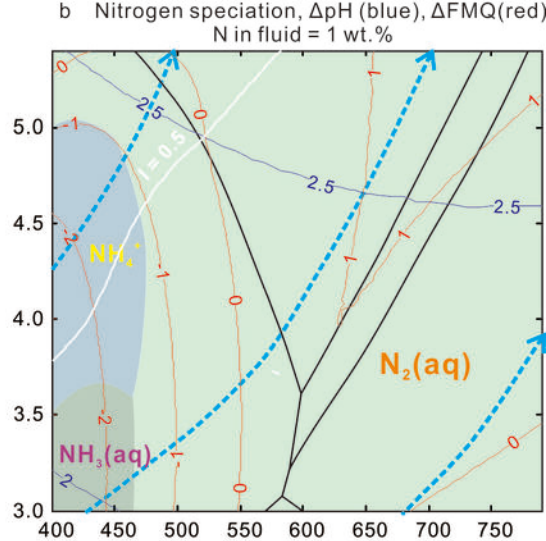
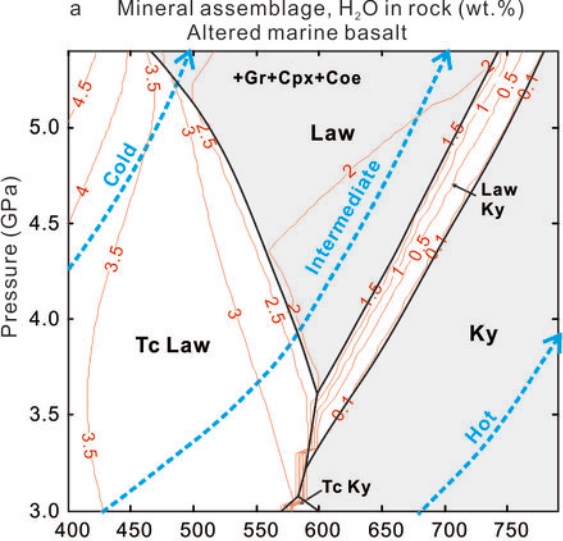


Figure 3.

